Optics Letters

Enhanced Fano resonance in a non-adiabatic tapered fiber coupled with a microresonator

Kun Zhang,[1,2] Yue Wang,[1] and Yi-Hui Wu[1,*]

[1]State Key Laboratory of Applied Optics, Changchun Institute of Optics, Fine Mechanics and Physics, Chinese Academy of Sciences, Changchun 130033, China
[2]University of Chinese Academy of Sciences, Beijing 100049, China
*Corresponding author: yihuiwu@ciomp.ac.cn

Received 1 June 2017; revised 27 June 2017; accepted 1 July 2017; posted 3 July 2017 (Doc. ID 297217); published 25 July 2017

We achieved enhanced Fano resonance by coupling a bottle resonator with a special non-adiabatic tapered fiber, where there is a high intensity distribution ratio between high-order and fundamental modes in the tapered region, as well as single mode propagation in the waist region. The resonance line shape is theoretically proved to be related to the intensity distribution ratio of the two fiber modes and their phase shift. An enhanced Fano line shape with an extinction ratio over 15 dB is experimentally reached by improving the intensity distribution ratio and tuning the phase shift. The results can remarkably improve the sensitivity of whispering-gallery mode microresonators in the field of optical sensing.

OCIS codes: (140.3948) Microcavity devices; (230.3990) Micro-optical devices; (280.4788) Optical sensing and sensors.

https://doi.org/10.1364/OL.42.002956

Fano resonance originates from the interference between discrete excited states and a continuum of states in the quantum system [1,2]. Compared with Lorentz resonance, Fano is characterized by asymmetric line shape, which causes significant changes in transmittance and reflectance over a narrow spectrum range. This is important for optical sensing and optical signal processing. A whispering-gallery mode (WGM) optical microresonator has high quality factor (Q-factor) and small mode volume [3], which can significantly enhance the interaction between light and matter. This makes it an excellent candidate in the aforementioned fields. Thus, it has been increasingly researched to achieve Fano resonance in a high Q-factor WGM resonator coupling system.

For a typical coupling system composed of a single mode waveguide and a WGM resonator, the transmission spectrum manifests itself as Lorentzian line shape, i.e., a state of this system. It requires another state, discrete or continuum, to produce a Fano line shape. Generally, a discrete state is produced in several methods, including introduction of another WGM with a higher Q-factor in the same resonator [4], indirect coupling with another resonator's mode through a waveguide [5–8], and nonlinear frequency conversion like four-wave mixing [9]. The continuum state is attained by doping the resonator with active rare-earth ions [10,11] or exciting the localized surface plasmon in a surface-modified resonator by metal nanoparticles [12]. In Refs. [13–17], a continuum state is introduced by coupling the resonator with only one multimode waveguide, which is a simple method to achieve a wavelength-independent Fano line shape. Nevertheless, the passive methods make it hard to achieve an enhanced Fano resonance, i.e., the transmission of the system exceeds the unit significantly, which is beneficial to the optical sensing.

In this Letter, an enhanced Fano resonance is experimentally observed by coupling a bottle WGM resonator with a special non-adiabatic multimode tapered fiber. We analyze the coupling characteristics between two fiber modes and one WGM using the coupled mode theory and demonstrate that a high intensity distribution ratio and proper phase shift help achieve the enhanced Fano resonance. Moreover, a Fano line shape with ultra-high transmissivity is experimentally attained and theoretically well fitted. This is highly beneficial to improving the WGM-based sensing performance.

A non-adiabatic tapered fiber is a multimode waveguide in the near-waist region, and modes in tapered fibers can be determined during the pulling process [18,19]. When multiple fiber modes couple with a resonance mode, there is a phase shift that causes the Fano resonance. For simplicity, only two fiber modes are considered, as shown in Fig. 1(a). A non-adiabatic tapered fiber consists of the fundamental mode (mode 1) and a high-order mode (mode 2), and they couple with a single WGM in a microresonator simultaneously, but only mode 1 is allowed to pass through the waist region and can be finally detected. In this situation, assuming that the coupling strength between two fiber modes is weak, the coupled mode equation [20] for the optical field inside the resonator can be expressed by

$$\frac{da}{dt} = -\left(i\Delta\omega + \frac{\kappa_0 + \kappa_{ex1} + \kappa_{ex2}}{2}\right)a + \sqrt{\kappa_{ex1}}E_1 + \sqrt{\kappa_{ex2}}e^{i\Delta\varphi}E_2, \quad (1)$$

where α is the amplitude of the WGM, and $\Delta\omega = \omega - \omega_0$ is the frequency detuning between the resonance and the incident light. κ_0 denotes the decay rate due to cavity intrinsic loss, $\kappa_{ex1}(\kappa_{ex2})$ denotes the decay rate due to external coupling to

mode 1(2). $|E_1|^2(|E_2|^2)$ is the input power of mode 1 (mode 2), $|\sqrt{\kappa_{ex1}}E_1|^2$ ($|\sqrt{\kappa_{ex2}}E_2|^2$) is the power coupled into the WGM from the mode 1 (mode 2), and $\Delta\varphi$ is the phase shift between them. With the steady state expression of α, we can have the output $E_{out} = E_1 - \sqrt{\kappa_{ex1}}\alpha$, and, further, the normalized transmission spectrum of mode 1 can be derived as

$$T = \left| \frac{i\Delta\omega + \frac{\kappa_0 - \kappa_{ex1} + \kappa_{ex2}}{2} - \sqrt{\kappa_{ex1}\kappa_{ex2}}e^{i\Delta\varphi}\frac{E_2}{E_1}}{i\Delta\omega + \frac{\kappa_0 + \kappa_{ex1} + \kappa_{ex2}}{2}} \right|^2. \quad (2)$$

T can be analogized to the classical Fano formula [21], as shown in Fig. 1(b), where $q = -2\sqrt{(\kappa_{ex1}\kappa_{ex2})}/\Gamma \cdot (E_2/E_1) \cdot \sin(\Delta\varphi)$ is the asymmetry parameter, and $\varepsilon = \Delta\omega/(\Gamma/2)$ is the normalized frequency detuning. $b = [(\kappa_0 - \kappa_{ex1} + \kappa_{ex2})/\Gamma - 2\sqrt{(\kappa_{ex1}\kappa_{ex2})}/\Gamma \cdot (E_2/E_1) \cdot \cos(\Delta\varphi)]^2$ is positive because it mainly influences the amplitude of the resonance, and $\Gamma = (\kappa_0 + \kappa_{ex1} + \kappa_{ex2})$ is the full width at half-maximum of the resonance. In this system, Fano resonance can be explained as interference between two associated discrete states (the same WGM excited by mode 1 and mode 2, respectively) and a continuum (mode 1). From the viewpoint of the asymmetry parameter q, the phase shift $\Delta\varphi$ makes the resonance line shape vary periodically by 2π, and the intensity distribution ratio E_2/E_1 determines the maximum degree of asymmetry. The dependences on these parameters are demonstrated in Figs. 1(c)–1(d). When $\Delta\varphi$ is an integer multiple of π, the output shows a symmetric Lorentzian line shape (blue and red lines), and it can be tuned between a dip and a peak by changing the intensity distribution ratio. In other cases, the line shape behaves like an asymmetric Fano (yellow and orange lines). It is noted that if the condition $|\sqrt{\kappa_{ex1}}E_1| < |\sqrt{\kappa_{ex2}}E_2|$ is satisfied, the Fano line shape becomes sharper than that under the condition $|\sqrt{\kappa_{ex1}}E_1| > |\sqrt{\kappa_{ex2}}E_2|$. This, thus, provides us a method to produce an enhanced Fano line shape.

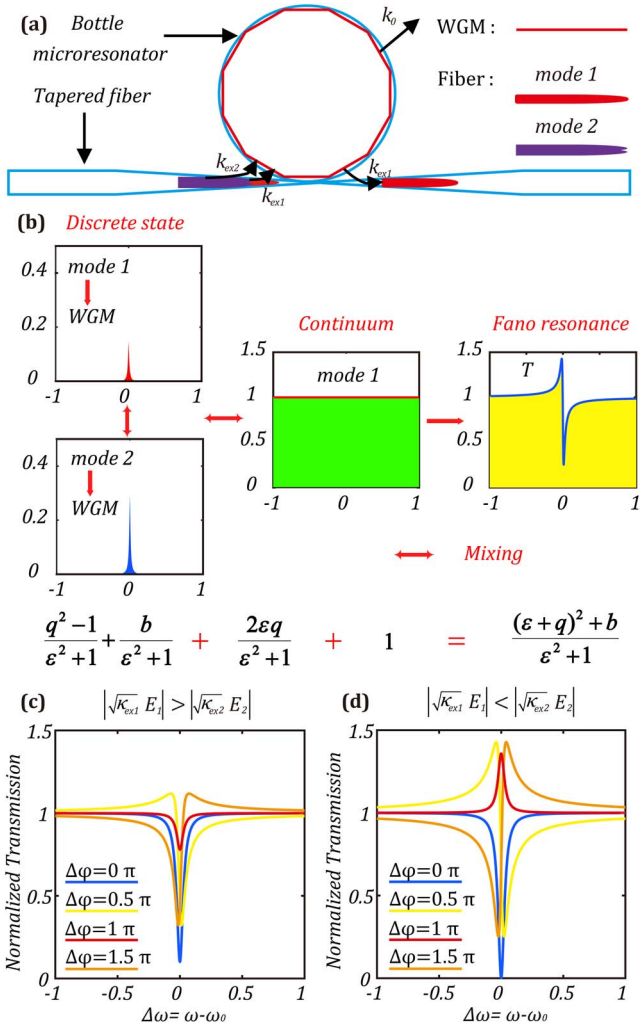

Fig. 1. (a) Schematic of two optical fiber modes coupled with one WGM. (b) Illustration of the Fano resonance formation from the classical viewpoint [1,21]. (c) Four types of line shapes with the different phase shifts on the $|\sqrt{\kappa_{ex1}}E_1| > |\sqrt{\kappa_{ex2}}E_2|$ condition, where (d) is the same as (c), but on the $|\sqrt{\kappa_{ex1}}E_1| < |\sqrt{\kappa_{ex2}}E_2|$ condition. Note that $\kappa_{ex2} = 2\kappa_{ex1} = \kappa_0$, $E_2 = 0.5E_1$ for (c), and $\kappa_{ex2} = 2\kappa_{ex1} = \kappa_0$, $E_2 = E_1$ for (d).

To experimentally demonstrate these rules, we built the setup, as shown in Fig. 2(a). An add–drop coupling configuration was adapted [22] for its convenience in monitoring the WGM directly. It included a bottle resonator produced by fusing a fiber (Corning SMF–28e+), a non-adiabatic tapered fiber (fiber 1) as the input-through fiber, and an adiabatic tapered fiber (fiber 2) as the add–drop fiber. These two fibers were positioned on a pair of defocus positions of the bottle [23,24]. A narrow linewidth (<200 kHz) tunable laser excited WGMs through fiber 1, and we detected the outputs from the drop and through ports simultaneously.

For a tapered fiber with high transmission, the amplitude of the fundamental mode E_1 is the highest, but κ_{ex1} is less than κ_{ex2} due to more extended field distribution of high-order mode [14]. To achieve enhanced Fano line shape, E_1 should be as small as possible to satisfy the condition $|\sqrt{\kappa_{ex1}}E_1| < |\sqrt{\kappa_{ex2}}E_2|$. It has been proved that tapered fiber with a large cone angle has a low transmission rate, and this was attained by misaligning the fiber holders by about 2 mm before pulling here.

The transmission of fiber 1 as a function of pulling length is shown in Fig. 2(b). In the pulling process, the fundamental mode begins to convert to high-order mode from point A, and, further, its energy dissipates to the surroundings because of a sharp drop in the core radius from point B. At point C, the core becomes too thin to confine the mode, therefore, the cladding becomes the new core and air becomes the new cladding, producing a multimode fiber. As the fiber becomes thinner, the high-order mode degenerates into several modes, and they interfere with each other, especially with the fundamental mode, resulting in serious oscillations from points C to E. The stepwise drop of the transmission denotes the cutoff of each high-order mode, as shown in the insert. After point E, the waist diameter meets the single mode condition again. Oscillations, thus, disappear, and the final rate decreases to 32%. Experimentally, the bottle is coupled with the multimode region around point D. Furthermore, serving as the add–drop ports, fiber 2 is an adiabatic tapered fiber with a transmission rate over 95%.

The enhanced Fano line shape is characterized in two perspectives. First, the response of the through port in a wide spectrum range from 1546 to 1550 nm is examined in Fig. 2(c). It is evident that most of the resonances manifest themselves as Fano line shapes, and they vary with wavelength, as presented in the inset of Fig. 2(c). It gives four states, including Fano line

shape with a left-side shoulder (L-Fano), Lorentzian peak, Fano line shape with a right-side shoulder(R-Fano), and Lorentzian dip, respectively. This change is attributed to the fact that the phase shift between the two fiber modes depends on incident light wavelength. In addition, it is predicted that this periodic change will be appropriate to the whole spectrum range.

Second, the tunability of the Fano line shape under a certain wavelength is demonstrated by changing the relative position between the fiber 1 and the bottle. To achieve stable tuning, fiber 1 has contact with the bottle surface. We started from a Lorentzian dip and shifted the fiber slightly along a positive z direction, where the fiber diameter decreases. The line shapes at seven positions were recorded, as shown in Fig. 3(a). It evolves from a Lorentzian dip to a R-Fano, and then becomes a Lorentzian peak followed by L-Fano; finally, it goes back to the Lorentzian dip. The period is about 64 μm, which is far beyond the periods reported in Refs. [9,13]. This is because the diameter in the coupling region is bigger here, which means that the two fiber modes have closer propagation constants [18]. Clearly, the evolutions are well fitted with the theoretical transmission, i.e., Eq. (2), using the least squares method. The errors may be due to the involvement of other WGMs, and the slight changes of coupling parameters when moving fiber 1. Here, we attribute this periodical line shape evolution to one WGM coupling with two fiber modes rather than three or more modes, as illustrated in Ref. [13]. This is because the transmission line shape is related to the fiber mode's intensity. If the third fiber mode's intensity E_3 is small, i.e., $E_3 \ll \min\{E_1, E_2\}$, the transmission line shape will be slightly modified only as the experimental results, but with the increase of E_3, the transmission will maintain a Fano line shape and present more complex profile evolution. The exact and flexible tuning of Fano shows the dependences of the line shape on the parameters of the coupling system, and it provides us an approach of reaching the best performance of a sensor. This enriches the sensing mechanisms, from simply monitoring the shift of the resonance peak to the evolution of the line shape.

Moreover, whatever the line shapes of the through port, the drop port outputs a Lorentzian peak, as shown in Fig. 3(b).

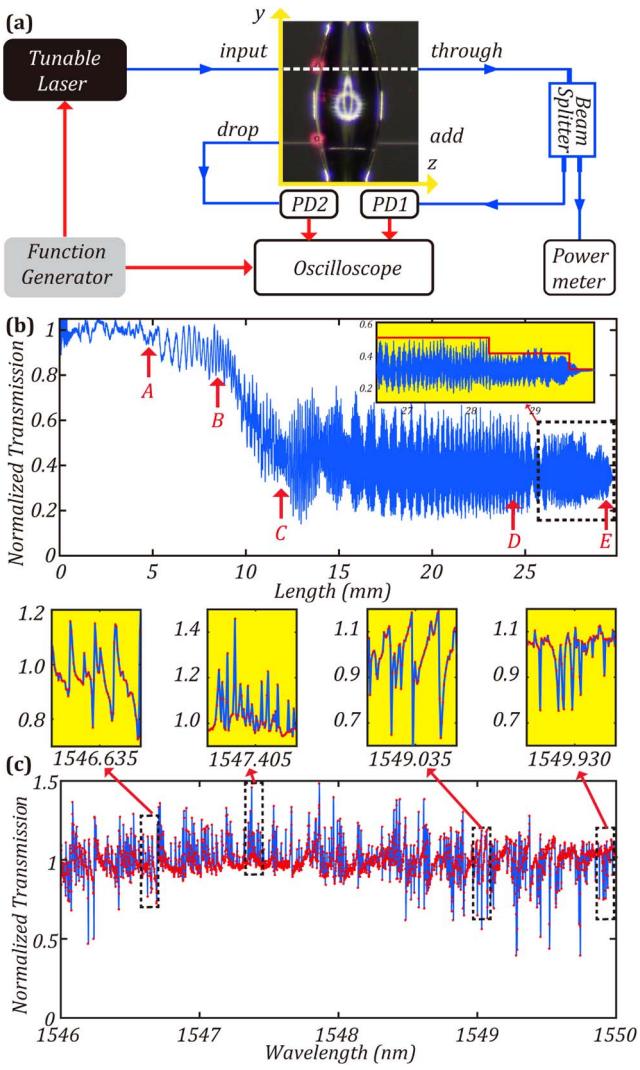

Fig. 2. (a) Schematic diagram of the experimental setup. PD, photo detector. The bottle resonator is photographed when coupled with taper fibers at 785 nm, and two red spots correspond to two defocus points of the bottle. The bottle is 115 μm in radius, 0.023 μm^{-1} in curvature, and the Q-factor is on the order of 1×10^6. Despite the introduction of fiber 2, the experimental results do not violate the theoretical model because fiber 2 just increases the loss of the resonator. The dot line indicates the position of fiber 1. (b) Normalized transmission of fiber 1 in the experiment detected at 1550 nm. (c) Normalized transmission from 1546 to 1550 nm of the through port, and four different line shapes are zoomed in the insets.

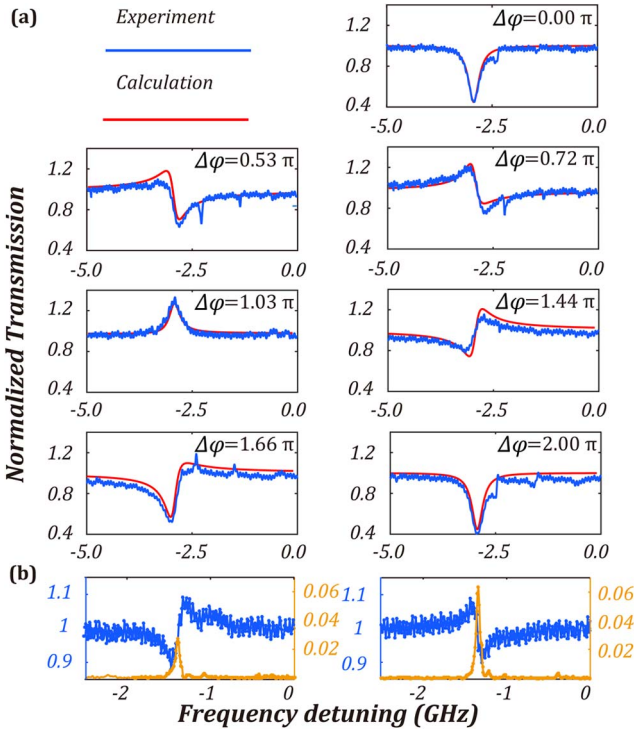

Fig. 3. (a) Tunable Fano line shapes in the through port around 1550 nm. They correspond to seven different coupling positions denoted by 0, 17, 23, 33, 46, 53, and 64 μm, and the normalized phases are 0, 0.53π, 0.72π, 1.03π, 1.44π, 1.66π, 2π, respectively. The fitting parameters are $E_2/E_1 = 0.62$, $\kappa_{ex1} = 0.23\kappa_0$, $\kappa_{ex2} = 3.56\kappa_0$, $\kappa_0 = 4.05 \times 10^8$, and the loaded Q-factor is 6.3×10^5. Though phase shift changes the line shape, it has no influence on the Q-factor. (b) Transmission in the through (blue line) and drop (yellow line) ports. Note that the WGM in (b) differs from (a).

This is because the WGM results from interference between optical fields coupled from two fiber modes, and its amplitude varies with the periodically constructive and destructive interference. This feature further indicates that only one WGM is involved in producing a Fano line shape, and each WGM of the resonator can be a Fano candidate.

Here, a tapered fiber with normalized transmission of 3% was obtained by enhancing the misalignment before pulling, and an enhanced Fano line shape with normalized transmission as high as 14 is observed, as shown in Fig. 4(a). This is 2.5 times higher than the theoretical predictions in Ref. [25], which utilizes an active element. The corresponding extinction ratio is 15.26 dB, and the slope rate reaches 35.5 dB/GHz. The sensitivity of this line shape, according to $S = |dT/d\omega|$ [26,27], reaches 4.5, as shown in Fig. 4(b), which is enhanced by nearly 30 times compared with a Lorentzian line shape of the same Q-factor. Furthermore, we find that the most sensitive wavelength can be shifted flexibly by changing $\Delta\varphi$; it locates at the region where the transmission sharply drops from the maximum to its minimum (for $0 < \Delta\varphi < \pi$) or increases from the minimum to its maximum (for $\pi < \Delta\varphi < 2\pi$). This shows potential advantages for WGM-based sensing, and it is expected to have a higher slope by exactly tuning the mode distribution and the coupling conditions, such as selective mode coupling by writing grating on the surface of the resonator [28] or modifying the tapered fiber with nano particles [29]. In addition, it is intriguing to involve more WGMs and fiber modes. For example, it is anticipated to observe an enhanced electromagnetically induced transparency phenomenon [27,30] by coupling two fiber modes with two WGMs in a bottle resonator, and this will be further exampled.

In summary, a tunable enhanced Fano line shape is experimentally achieved by coupling two fiber modes from a special non-adiabatic tapered fiber with a single WGM in a bottle resonator. We find that the normalized transmission is analogous to the classical Fano formula, where the asymmetric parameter q depends on the intensity distribution ratio of fiber modes and their phase shift, and demonstrate that its profile can be modified periodically between Fano and Lorentzian. By improving the intensity distribution ratio in an ultra-low transmission tapered fiber, we experimentally achieve a Fano line shape with an extinction ratio over 15 dB. With this method, the sensing performance can be improved remarkably without depending on a certain wavelength. Further attention should be paid to optimize the taper fiber profile, i.e., modifying mode distribution in the fiber to achieve selective mode coupling.

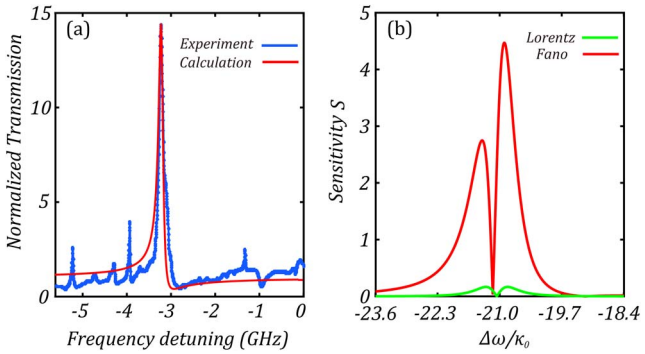

Fig. 4. (a) Enhanced Fano resonance around 1550 nm. The fitting parameters are $E_2/E_1 = 6.67$, $\kappa_{ex1} = 0.41\kappa_0$, $\kappa_{ex2} = 3.58\kappa_0$, $\kappa_0 = 1.52 \times 10^8$, and $\Delta\varphi = 0.66\pi$. The loaded Q-factor is 1.6×10^6, and this is on the same order as that in Refs. [12,15]. (b) Sensitivity S (in units of κ_0) as a function of the detuning $\Delta\omega/\kappa_0$ for two configurations: the Fano resonance from (a) (red line) and a Lorentzian resonance with the same Q-factor (green line).

Funding. National High Technology Research and Development Program of China (2015AA042402); China-Israel International Science and Technology Cooperation Program (2015DFG02620).

Acknowledgment. The authors thank Xi Zhang, Dong Zhang in SIOM, Jie Zang in Shandong University, and Di-Chen Zhang.

REFERENCES

1. U. Fano, Phys. Rev. **124**, 1866 (1961).
2. A. E. Miroshnichenko, S. Flach, and Y. S. Kivshar, Rev. Mod. Phys. **82**, 2257 (2010).
3. K. J. Vahala, Nature **424**, 839 (2003).
4. B.-B. Li, Y.-F. Xiao, C.-L. Zou, Y.-C. Liu, X.-F. Jiang, Y.-L. Chen, Y. Li, and Q. Gong, Appl. Phys. Lett. **98**, 021116 (2011).
5. S. Fan, Appl. Phys. Lett. **80**, 908 (2002).
6. C.-Y. Chao and L. J. Guo, Appl. Phys. Lett. **83**, 1527 (2003).
7. Y.-F. Xiao, M. Li, Y.-C. Liu, Y. Li, X. Sun, and Q. Gong, Phys. Rev. A **82**, 065804 (2010).
8. B.-B. Li, Y.-F. Xiao, C.-L. Zou, X.-F. Jiang, Y.-C. Liu, F.-W. Sun, Y. Li, and Q. Gong, Appl. Phys. Lett. **100**, 021108 (2012).
9. Y. Zheng, J. Yang, Z. Shen, J. Cao, X. Chen, X. Liang, and W. Wan, Light Sci. Appl. **5**, e16072 (2016).
10. F. Lei, B. Peng, Ş. K. Özdemir, G. L. Long, and L. Yang, Appl. Phys. Lett. **105**, 101112 (2014).
11. X.-F. Liu, F. Lei, M. Gao, X. Yang, C. Wang, Ş. K. Özdemir, L. Yang, and G.-L. Long, Opt. Express **24**, 9550 (2016).
12. K. D. Heylman, N. Thakkar, E. H. Horak, S. C. Quillin, C. Cherqui, K. A. Knapper, D. J. Masiello, and R. H. Goldsmith, Nat. Photonics **10**, 788 (2016).
13. A. Chiba, H. Fujiwara, J. Hotta, S. Takeuchi, and K. Sasaki, Appl. Phys. Lett. **86**, 261106 (2005).
14. A. C. Ruege and R. M. Reano, J. Lightwave Technol. **27**, 2035 (2009).
15. A. C. Ruege and R. M. Reano, Opt. Express **17**, 4295 (2009).
16. D. Ding, M. J. A. de Dood, J. F. Bauters, M. J. R. Heck, J. E. Bowers, and D. Bouwmeester, Opt. Express **22**, 6778 (2014).
17. J. Liao, X. Wu, L. Liu, and L. Xu, Opt. Express **24**, 8574 (2016).
18. F. Orucevic, V. Lefèvre-Seguin, and J. Hare, Opt. Express **15**, 13624 (2007).
19. S. Ravets, J. E. Hoffman, L. A. Orozco, S. L. Rolston, G. Beadie, and F. K. Fatemi, Opt. Express **21**, 18325 (2013).
20. H. A. Haus, *Waves and Fields in Optoelectronics* (Prentice-Hall, 1984), p. 210.
21. I. Avrutsky, R. Gibson, J. Sears, G. Khitrova, H. M. Gibbs, and J. Hendrickson, Phys. Rev. B **87**, 125118 (2013).
22. M. Cai, G. Hunziker, and K. Vahala, IEEE Photon. Technol. Lett. **11**, 686 (1999).
23. M. Sumetsky, Opt. Lett. **29**, 8 (2004).
24. M. Pöllinger, D. O'Shea, F. Warken, and A. Rauschenbeutel, Phys. Rev. Lett. **103**, 053901 (2009).
25. Y. Zhao, C. Qian, K. Qiu, J. Tang, Y. Sun, K. Jin, and X. Xu, Sci. Rep. **6**, 33645 (2016).
26. Y.-F. Xiao, V. Gaddam, and L. Yang, Opt. Express **16**, 12538 (2008).
27. J. Li, R. Yu, C. Ding, and Y. Wu, Phys. Rev. A **93**, 023814 (2016).
28. D. C. Aveline, L. M. Baumgartel, G. Lin, and N. Yu, Opt. Lett. **38**, 284 (2013).
29. G.-G. Liu, Y.-H. Wu, K.-W. Li, P. Hao, and M. Xuan, Appl. Opt. **52**, 775 (2013).
30. Y. Wang, K. Zhang, S. Zhou, Y.-H. Wu, M.-B. Chi, and P. Hao, Opt. Lett. **41**, 1825 (2016).